# **EDGE ARTICLE**

# **Hybrid Ruthenium Halide Perovskites and Related Compounds**

Pratap Vishnoi,<sup>a</sup> Julia L. Zhuo,<sup>b</sup> T. Amanda Strom,<sup>a</sup> Guang Wu,<sup>c</sup> Stephen D. Wilson,<sup>b</sup>

Ram Seshadri, a,b,c and Anthony K. Cheethama,b,d

Received 00th January 20xx, Accepted 00th January 20xx

DOI: 10.1039/x0xx000000x

There has been a great deal of recent interest in extended compounds containing  $Ru^{3+}$  and  $Ru^{4+}$  in light of their range of unusual physical properties. Many of these properties are displayed in compounds with the perovskite and related structures. Here we report an array of hybrid halide perovskites and related compounds of Ru:  $MA_2RuX_6$  (X = CI or Br),  $MA_2MRuX_6$  (M = Na, K or Ag; X = CI or Br) and  $MA_3Ru_2X_9$  (X = Br) based upon the use of methylammonium ( $MA = CH_3NH_3^+$ ) on the perovskite A site. The compounds  $MA_2RuX_6$  with  $Ru^{4+}$  crystallize in the trigonal space group  $R\overline{3}m$  and can be described as vacancy-ordered double-perovskites. The ordered compounds  $MA_2MRuX_6$  with  $M^{1+}$  and  $Ru^{3+}$  crystallize in a structure related to  $BaNiO_3$  with alternating  $MX_6$  and  $RuX_6$  face-shared octahedra forming linear chains in the trigonal  $P\overline{3}m$  space group. The compound  $MA_3Ru_2Br_9$  crystallizes in the orthorhombic Cmcm space group and displays pairs of face-sharing octahedra forming isolated  $Ru_2Br_9$  moieties with very short Ru-Ru contacts of 2.789 Å. The structural description, including the role of hydrogen bonding and dimensionality, as well as the optical and magnetic properties of these compounds are described. The magnetic behavior of all three classes of compounds is influenced by spin-orbit coupling and their temperature-dependent behavior has been compared with the predictions of the appropriate Kotani models.

### Introduction

Since the discovery of the remarkable optoelectronic properties of lead-based hybrid perovskite halides such as MAPbI<sub>3</sub> (MA = CH<sub>3</sub>NH<sub>3</sub>), 1-4 a great deal of recent interest has focused on related systems of general formula  $AMX_3$  (A = monovalent cation such as CH<sub>3</sub>NH<sub>3</sub>; *M* = bivalent metal ion such as Pb or Sn; X = halide such as Cl, Br or I). On account of the toxicity of Pb, there has also been a significant activity associated with perovskites based on other divalent metals, particularly Sn.5-10 In addition, simultaneous replacement of the divalent ion with a monovalent and a trivalent metal ions gives rise to double perovskites, A2MM'X6. Owing to the tuneability of M and the M', the hybrid double perovskites show great chemical diversity. For example, the neighbors of lead in the periodic table, such as Ag, Sb, Tl, and Bi have been employed for the synthesis of leadfree hybrid double perovskites, many of which show excellent optoelectronic and other properties. 11-14

Beyond hybrid double perovskites, the high level of interest in this area has led to significant activity in related perovskite chemistries, including the study of 1-D and layered hybrid structures. <sup>15–22</sup> There is also growing interest in hybrid *B*-site vacancy perovskite halides of general formula  $A_2MX_6$ , which are related to the well-known  $K_2PtCl_6$  structure. For example, the discovery of  $MA_2PtCl_6$  and related materials containing Pt(IV) and Sn(IV) has been recently reported. <sup>23–25</sup>  $MA_2Snl_6$  absorbs in the visible to the near-infrared regions of the solar spectrum. <sup>25</sup> Hybrid halide perovskites and related compounds, together with their structural relationships, are displayed schematically in **Fig. 1**.

In the present work, we extend the domain of hybrid halide perovskites to the study of ruthenium-containing compounds. There is an extensive literature on ruthenium oxide perovskites such as 3D ARuO<sub>3</sub> (A = Ca, Sr or Ba) and  $A_{n+1}Ru_nO_{3n+1}$  (A = Ca, Sr or Ba; n = 1, 2 or 3) type Ruddlesden-Popper structures. These oxides show a wide range of exciting properties, such as proposed spin-triplet superconductivity in Sr<sub>2</sub>RuO<sub>4</sub><sup>26,27</sup> and the coexistence of ferromagnetism and metallic conductivity in SrRuO<sub>3</sub>.<sup>28-30</sup> More recently, many Ru compounds have been studied in light of the interplay between spin-orbit coupling and electron correlation.<sup>31</sup> In particular, α-RuCl<sub>3</sub> has been suggested<sup>32</sup> to potentially host a Kitaev quantum spin liquid ground state<sup>33</sup> which may be relevant for quantum computing. New chemistry on this layered compound has been emerging apace. 34,35 There are a small number of inorganic ruthenium halides with perovskite-related structures such as K<sub>2</sub>RuCl<sub>6</sub>,<sup>36,37</sup> but very few hybrid halides of Ru have been reported.<sup>38,39</sup> The magnetic properties of these latter compounds have been investigated and their temperature- dependent magnetic moments are found be broadly in accord with the Kotani theory.40,41

Materials Research Laboratory, University of California, Santa Barbara, CA 93106, United States.

b. Materials Department, University of California, Santa Barbara, CA 93106, United States.

<sup>&</sup>lt;sup>c</sup> Department of Chemistry and Biochemistry, University of California, Santa Barbara, CA 93106, United States.

d. Department of Materials Science & Engineering, National University of Singapore, Singapore 117576

<sup>†</sup> Footnotes relating to the title and/or authors should appear here. Electronic Supplementary Information (ESI) available: CCDC 1982755 (1), 1982756 (2), 1982757 (3), 1982758 (4), 1982759 (5), 1982760 (6), 1982761 (7), 1982762 (8) and 1982763 (9). For ESI see DOI: 10.1039/x0xx00000x.

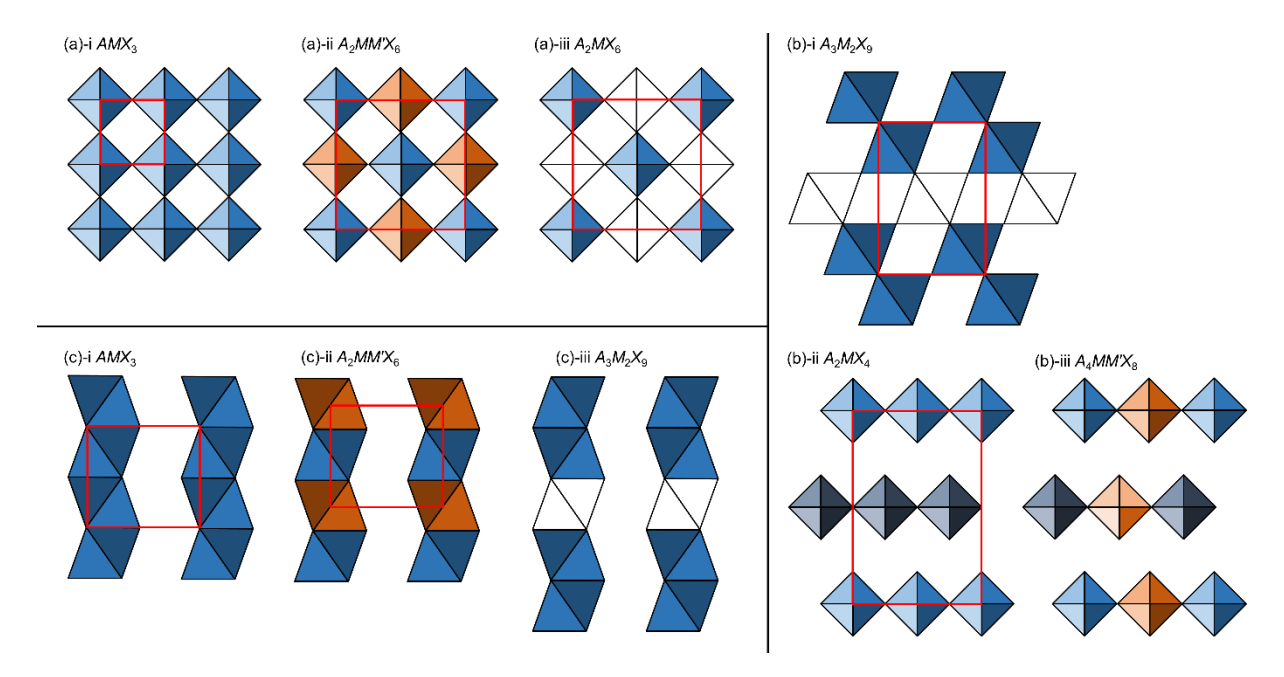


Fig. 1.

We describe here the discovery and characterization of nine methylammonium Ru halides belonging to three families:  $MA_2Ru^{IV}X_6$  (X = CI or Br), **1**, **2**;  $MA_2MRu^{III}X_6$  (M = Na, K or Ag; X = CI or Br), **3-8**; and  $MA_3Ru^{III}_2X_9$  (X = Br), **9**. The crystal structures and the optical and magnetic properties of these compounds have been determined and their behaviour is compared with related inorganic compounds that have been described in the literature.

## **Experimental Section**

# **Materials and Methods**

Methylammonium chloride (Sigma Aldrich), methylammonium bromide (Sigma Aldrich), NaCl (Merck), KCl (Merck), AgCl (Merck), NaBr (Merck), anhydrous RuCl $_3$  (Alfa Easar), 37 wt. % HCl in H $_2$ O (Merck), 48 wt. % HBr in H $_2$ O (Sigma Aldrich), 50 wt. % H $_3$ PO $_2$  in H $_2$ O (Sigma Aldrich) were purchased from commercial sources and used as received. All the compounds were synthesized hydrothermally in 23 mL Teflon-lined autoclave. The crystals were separated by filtration, washed several times with ethanol and dried under vacuum. Details for the syntheses of  $\bf 1$  to  $\bf 9$  are given in the Supplementary Information.

#### Single crystal X-ray diffraction

Room temperature single-crystal X-ray diffraction data were collected on a Bruker Kappa Apex II diffractometer equipped with an APEX II CCD detector and a TRIUMPH monochromator with Mo-K $\alpha$  X-ray source (wavelength = 0.71073 Å) in  $\omega$ -scan mode. The data collection and integration were carried out on APEX3 software. The structures were solved by direct methods and refined by full-matrix least-squares on  $F^2$  by using SHELXL-2014 program package. The non-hydrogen atoms were

located from the electron density found in the difference maps and refined anisotropically. The hydrogen atoms of methylammonium cations were placed in their geometrically idealized positions and refined with isotopic parameters as riding atoms. The structures were drawn from CIFs by using VESTA (version 3) software.

#### **Powder X-ray diffraction**

Powder diffraction data were on a Panalytical Empyrean powder diffractometer equipped with a Cu-K $\alpha$  X-ray source (wavelength = 1.54056 Å). The experimental PXRD patterns were compared with the patterns simulated from the CIF of single-crystal X-ray diffraction data (see Supplementary Information) in order to verify the phase purity of the bulk samples (Figs. S1-S9, supporting information).

#### Thermogravimetric analysis (TGA)

TGA of all compounds was carried out under continuous flow of nitrogen gas (flow rate; 25 mL/minute) on a Discovery TGA instrument (TA Instruments). The samples (5-6 mg) were heated in aluminum crucibles at a temperature ramp rate of 10 °C min<sup>-1</sup>. The details are given in the Supplementary Information, **Figs. S10-S18**.

## **Optical properties**

Diffuse reflectance spectra were measured in the wavelength range of 220–2600 nm on a Shimadzu UV-3600 UV–vis–NIR spectrometer. BaSO $_4$  (Sigma Aldrich) was used as the reference (100% reflectance) as well as for dilution of the samples. The samples were prepared by mixing each compound with BaSO $_4$  in a 1:3 ratio. The diffuse reflectance data were converted to absorbance by using Kubelka–Munk (K-M) expression,

$$\frac{k}{s} = \frac{(1-R)^2}{(2R)}$$

where k is the absorption coefficient, s is the scattering coefficient and R is the reflectance. It is generally assumed that s is a constant and it is independent of wavelength. Therefore, the k/s term is assumed to be equivalent to the absorption coefficient.

#### **Magnetic properties**

Magnetic susceptibility measurements were collected for compounds **1**, **3** and **9** on a Quantum Design MPMS3 SQUID magnetometer. In each case, approximately 15 mg of powder sample was mounted on a brass holder in plastic caps. Zero field-cooled (ZFC) and field-cooled (FC) susceptibility versus temperature measurements were performed in the 2 to 300K range. We used the Curie law,

$$m_{eff} = \sqrt{\frac{3k_B}{N_A\mu_B^2}\chi T}$$

to transform the molar magnetic susceptibilities ( $\chi$ ) into the effective magnetic moments ( $m_{\rm eff}$ ), where  $k_{\rm B}$  is the Boltzmann constant,  $\chi$  is the molar susceptibilities, T is the temperature,  $N_{\rm A}$  is Avogadro's number and  $\mu_{\rm B}$  is Bohr magneton.

#### **Results and Discussion**

## **Synthesis**

MA<sub>2</sub>Ru<sup>IV</sup>Cl<sub>6</sub> (1), MA<sub>2</sub>Ru<sup>IV</sup>Br<sub>6</sub> (2), MA<sub>2</sub>NaRu<sup>III</sup>Cl<sub>6</sub> (3), MA<sub>2</sub>AgRu<sup>III</sup>Cl<sub>6</sub> (4),  $MA_2KRu^{|||}Cl_6$  (5),  $MA_2NaRu^{|||}Br_6$  (6),  $MA_2AgRu^{|||}Br_6$  (7), MA<sub>2</sub>KRu<sup>III</sup>Br<sub>6</sub> (8) and MA<sub>3</sub>Ru<sup>III</sup><sub>2</sub>Br<sub>9</sub> (9) have been synthesized solvothermally and their structures have been determined by single-crystal X-ray diffraction. The compounds 1 and 2 were obtained from the reaction of RuCl<sub>3</sub> with MA·Cl in aqueous HCl and MA·Br in aqueous HBr, respectively. During the reactions in the acidic media, Ru<sup>3+</sup> oxidized to Ru<sup>4+</sup> and these ions were utilized in the formation of 1 and 2. In the cases of the compounds 3-8, however, where the simultaneous incorporation of  $M^+$  and  $Ru^{3+}$  ions is necessary to form the structures, the oxidation of Ru<sup>3+</sup> needed to be suppressed. This was achieved by using stoichiometric quantities (one equivalent relative to the RuCl<sub>3</sub>) of hypophosphorous acid (H<sub>3</sub>PO<sub>2</sub>). The diruthenium compound, MA<sub>3</sub>Ru<sub>2</sub>Br<sub>9</sub> (9), was obtained along with 8 from the reaction of methylammonium bromide, KCl, RuCl<sub>3</sub> and H<sub>3</sub>PO<sub>2</sub> in HBr. The details of X-ray data collection and structure refinement are provided in Tables S1 and the selected bond distances are listed in Table S2. The selected bond angles are given in Tables S3-S6.

## The vacancy-ordered double perovskites, 1 and 2

Compounds **1** and **2** are isostructural and crystallize in the rhombohedral space group,  $R\overline{3}m$  (**Table 1**) as reported previously for the case of MA<sub>2</sub>Ptl<sub>6</sub>.<sup>24</sup> **Fig. 2** shows the unit cells of **1** and **2**. The compounds contain isolated  $[RuX_6]^{2-}$  octahedra together with methylammonium cations in a motif. The

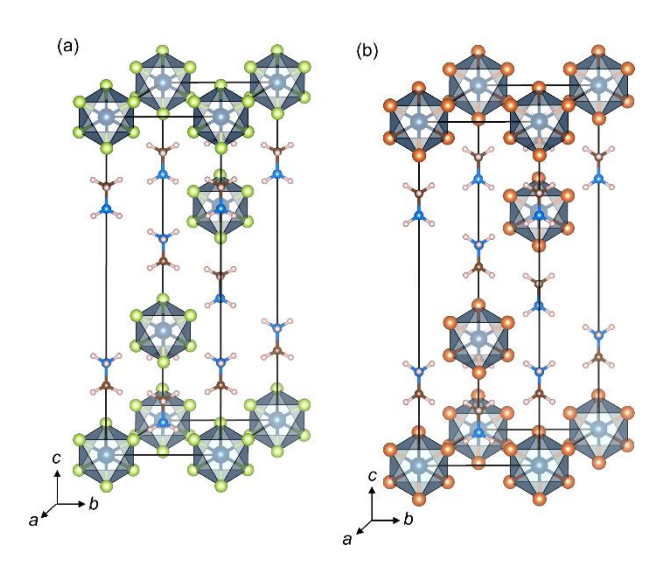


**Fig. 2.** Single-crystal structures (unit cells) of  $MA_2RuX_6$ . (a)  $MA_2RuCl_6$  (1). (b)  $MA_2RuBr_6$  (2). The isolated octahedra show  $RuCl_6$  and  $RuBr_6$  units. Methylammonium cations are present in the space between the octahedra in a head-to-tail orientation.

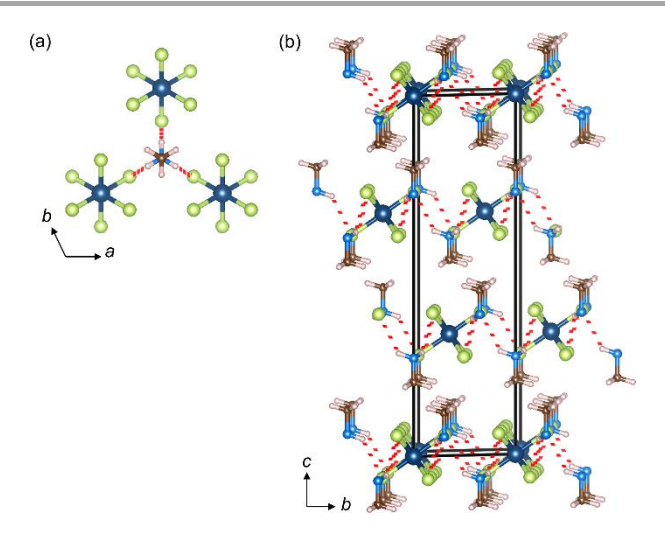


**Fig. 3.** Hydrogen bond interactions in  $MA_2RuCl_6$  (1). (a) The ball and stick model of three  $RuCl_6$  octahedra connected with a methylammonium cation by hydrogen bonds. The red dotted bonds show hydrogen bond interactions. (b) The packing diagram shows layer formation due to hydrogen bonds in the ab-plane.

structures are very similar to the vacancy-ordered double perovskites such as  $K_2RuCl_6$  with  $A_2MX_6$  as the structure type (**Fig. 1**). Unlike the cubic  $K_2RuCl_6$ , however, **1** and **2** lack a 4-fold symmetry axis due to a rhombohedral distortion that is caused by the alignment of the methylammonium cations. The Ru-Cl and Ru-Br bond distances [2.327(1) Å and 2.483(1) Å, respectively] are similar to those in other low-spin  $d^4$  Ru<sup>4+</sup> halides with octahedral coordination (**Table S2**). The bond angles within the Ru $X_6$  octahedra are extremely close to 90° and 180°, though this is not required by the crystal symmetry (**Table S3**). We ascribe the regularity of the Ru $X_6$  octahedra to the very high ligand field stabilization energy associated with the low spin  $d^4$  configuration of octahedral Ru<sup>4+</sup>.

Table 1. Structural properties of Ru Halides.

Compounds	Crystal symmetry	Unit cell dimensions (Å) and volumes (ų)	Structure type <sup>a</sup>
$MA_2RuCl_6$ (1)	Trigonal, $R\overline{3}m1$ (# 166)	a = b = 6.9935(3); $c = 21.9740(12)$ ; $V = 930.74(9)$	(a)-iii <i>A</i> <sub>2</sub> <i>MX</i> <sub>6</sub>
$MA_2RuBr_6$ (2)	Trigonal, $R\overline{3}m1$ (# 166)	a = b = 7.3485(10); $c = 22.376(4)$ ; $V = 1046.4(3)$	(a)-iii <i>A</i> <sub>2</sub> <i>MX</i> <sub>6</sub>
$MA_2NaRuCl_6$ (3)	Trigonal, $P\overline{3}m1$ (# 164)	a = b = 7.2493(9); $c = 6.7926(8)$ ; $V = 309.14(8)$	(c)-ii <i>A</i> <sub>2</sub> <i>MM'X</i> <sub>6</sub>
$MA_2AgRuCl_6$ (4)	Trigonal, $P\overline{3}m1$ (# 164)	a = b = 7.237(5); $c = 6.936(5)$ ; $V = 314.6(5)$	(c)-ii A <sub>2</sub> MM'X <sub>6</sub>
$MA_2KRuCl_6$ (5)	Trigonal, $P\overline{3}m1$ (# 164)	a = b = 7.181(5); $c = 7.366(5)$ ; $V = 329.0(5)$	(c)-ii <i>A</i> <sub>2</sub> <i>MM'X</i> <sub>6</sub>
$MA_2NaRuBr_6$ (6)	Trigonal, $P\overline{3}m1$ (# 164)	a = b = 7.561(5); $c = 7.105(5)$ ; $V = 351.8(5)$	(c)-ii <i>A</i> <sub>2</sub> <i>MM'X</i> <sub>6</sub>
MA <sub>2</sub> AgRuBr <sub>6</sub> ( <b>7</b> )	Trigonal, $P\overline{3}m1$ (# 164)	a = b = 7.516(5); $c = 7.032(4)$ ; $V = 344.1(5)$	(c)-ii <i>A</i> <sub>2</sub> <i>MM'X</i> <sub>6</sub>
$MA_2KRuBr_6$ (8)	Trigonal, $P\overline{3}m1$ (# 164)	a = b = 7.4892(17); c = 7.3894(18); $V = 358.93(18)$	(c)-ii <i>A</i> <sub>2</sub> <i>MM'X</i> <sub>6</sub>
$MA_2Ru_2Br_9$ (9)	Orthorhombic, Cmcm (# 63)	a = 7.3797(16); $b = 15.167(4)$ ; $c = 18.419(5)$ ; $V = 2061.6(9)$	(c)-iii $A_3M_2X_9$

<sup>&</sup>lt;sup>a</sup> Different structure types are shown in Fig. 1.

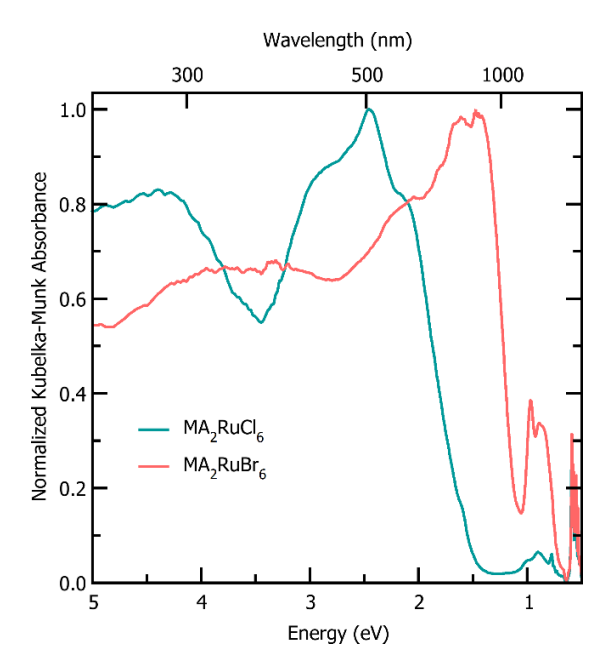
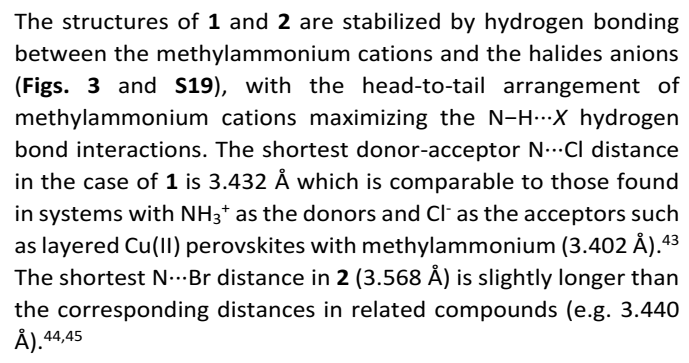


**Fig. 4.** Kubelka-Munk absorption spectra of  $MA_2RuCl_6$  (1) and  $MA_2RuBr_6$  (2) obtained from the Kubelka-Munk transformation of the diffuse reflectance data.



Compounds **1** and **2** show broad optical absorption spanning almost entire ultraviolet and visible region, and these Ru<sup>4+</sup> compounds appear black. Compound **1** shows two broad absorption bands centered around 4.43 and 2.43 eV (**Fig. 4**) which can be ascribed to ligand to metal charge transfer

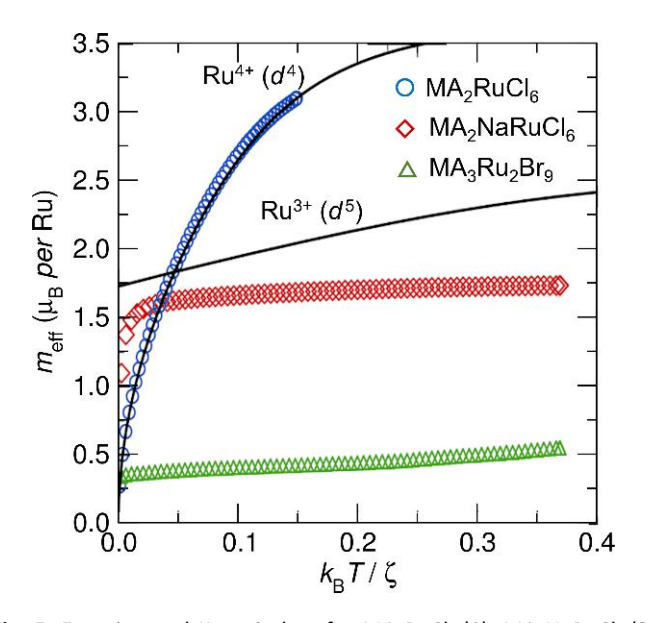


**Fig. 5.** Experimental Kotani plots for  $MA_2RuCl_6$  (1),  $MA_2NaRuCl_6$  (3) and  $MA_3Ru_2Br_9$  (9). For comparison, the theoretical Kotani plots for  $Ru^{+4}$  ( $d^4$ ) and  $Ru^{3+}$  ( $d^5$ ) single ions are given as the black lines.

(LMCT).<sup>46</sup> Due to the strong oxidizing nature of Ru<sup>4+</sup>, the symmetry allowed charge transfer bands obscure the weak bands arising from *d-d* transitions. The spectrum of **2** is slightly broadened and shifted to the red due to the lower electron affinity of Br compare to Cl. The LMCT absorption bands are positioned around 3.54 and 1.55 eV in the case of **2**. The multiple bands observed below 1.0 eV nm are due to the C-H overtones of the methylammonium cation, which was confirmed by measuring the spectrum of methylammonium chloride (**Fig. S20**).

The magnetic susceptibility measurements on **1** enabled us to calculate the effective magnetic moment as a function of temperature for this compound. Due to the isolated and undistorted nature of the RuCl<sub>6</sub> octahedra in MA<sub>2</sub>RuCl<sub>6</sub> and the intermediate strength of the spin-orbit coupling in Ru<sup>4+</sup>, at these temperatures we expect these compounds to exhibit single-ion

behaviour without the influence of exchange interactions. This behaviour was first described quantitatively by Kotani for an octahedral crystal field environment and follows a series of universal curves that depend on the d electron configuration when plotted against the unitless quantity  $k_{\rm B}T/\xi$  (where  $\xi$  is the spin-orbit coupling constant). The theoretical dependencies of  $m_{\rm eff}$  versus  $k_{\rm B}T/\xi$  are shown as solid black lines for low spin  $d^4$  Ru<sup>4+</sup> and low spin  $d^5$  Ru<sup>3+</sup> in **Fig. 5**. The experimental data for **1** are in excellent agreement with the Kotani plot calculated using a spin-orbit coupling constant  $\xi$  of 1400 cm<sup>-1</sup>. This value is consistent with the measurements on other low spin  $d^4$  Ru<sup>4+</sup> compounds such as  $({\rm NH_4})_2{\rm RuCl_6},^{38}$  and  ${\rm K_2RuCl_6},^{47}$  At low temperatures, the effective moment falls sharply to the ground state J=0. There is no evidence for deviations due to coupling between the widely spaced Ru<sup>4+</sup> ions.

#### MA<sub>2</sub>MRuX<sub>6</sub> compounds containing infinite chains

The six MA<sub>2</sub>M'Ru<sup>III</sup>X<sub>6</sub> compounds share the same general formula as the hybrid 3D double perovskites,  $A_2M^{\prime}M^{\prime\prime\prime}X_6$ , such as MA<sub>2</sub>KBiCl<sub>6</sub>,<sup>48</sup> MA<sub>2</sub>KGdCl<sub>6</sub>,<sup>49</sup> MA<sub>2</sub>KYCl<sub>6</sub>,<sup>49</sup> MA<sub>2</sub>AgBiBr<sub>6</sub>,<sup>12</sup> MA<sub>2</sub>TlBiBr<sub>6</sub>, <sup>11</sup> and MA<sub>2</sub>AgSbl<sub>6</sub>. <sup>14</sup> However, their structures are entirely different. Compounds 3-8 crystallize in the trigonal space group,  $P\overline{3}m$ , and contain infinite face-sharing chains of octahedral RuX<sub>6</sub> and trigonal-antiprismatic (trigonally elongated pseudo-octahedra) MX<sub>6</sub> polyhedra, interspersed with MA cations (Figs. 6 and 7). Successive  $RuX_6$  octahedra are in a staggered conformation along the c-axis. A similar chain structure, MA<sub>2</sub>AgInBr<sub>6</sub>, was recently reported which absorb in the ultraviolet region. 50 MA<sub>2</sub>AgInBr<sub>6</sub> comprises face-shared  $AgBr_6$  and  $InBr_6$  polyhedra. The chains of  $RuX_6$  and  $MX_6$ polyhedra in 3-8 are also reminiscent of Sr<sub>4</sub>PtO<sub>6</sub>, which contains chains of face-sharing octahedral PtO<sub>6</sub> and trigonal prismatic SrO<sub>6</sub>.51 Other examples of 1D perovskite-related transition metal oxides include Ca<sub>3</sub>NaRuO<sub>6</sub>,<sup>52</sup> Ca<sub>3</sub>NiMnO<sub>6</sub>,<sup>53</sup> Sr<sub>3</sub>ZnCoO<sub>6</sub>.<sup>54</sup> As in 1 and 2, the  $RuX_6$  octahedra in 3-8 are virtually undistorted, with all six Ru-X bonds of equal lengths and the X-Ru-X bond angles very close to 90° and 180° (Tables S2, S4 and S5). We again ascribe this finding to the very high ligand field stabilization energy associated with the low spin d<sup>5</sup> Ru<sup>3+</sup> configuration. The Ru-Cl bond distances in 3, 4, and 5 are comparable to those of β-RuCl<sub>3</sub> (2.351 Å), which has a TiCl<sub>3</sub>-type chain structure with face-sharing RuCl<sub>6</sub> octahedra.<sup>55</sup> The a and c axes of the unit cells of chlorides (3-5) are very similar because of the regularity of the RuCl<sub>6</sub> octahedra, so most of the cell volume changes due to the different sizes of the  $M^+$  ions are reflected in the lengths of the c-axes (the same is true of the bromides). This leads to the trigonal elongation of the MX6 octahedra in 3 - 8 along c-axes. Figs. 7c and 7d show the dependence of the unit cell volumes and intrachain  $\mbox{Ru}{\mbox{\scriptsize \cdots}}\mbox{Ru}$ distances (c-parameters) on the ionic radii of monovalent metals. All the M-X bonds of each compound are of equal length, but to compensate for the trigonal elongation along the c-axis, the X-M-X bond angles deviate significantly from 90° and 180° (Tables S2, S4 and S5). The methylammonium cations form N-H···X hydrogen bond interactions with the inorganic chains. The shortest donor...acceptor N...Cl distances in 3, 4 and 5 are

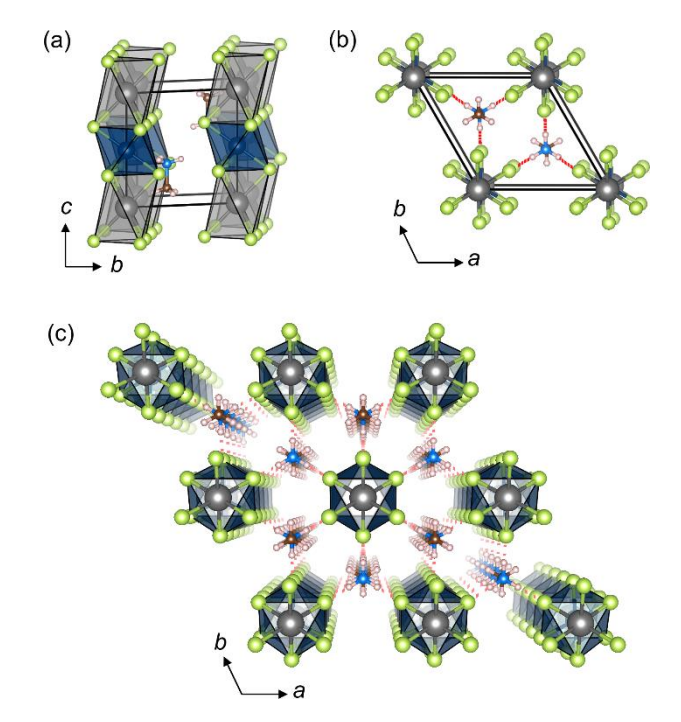


**Fig. 6.** Single-crystal X-ray structure of  $MA_2NaRuCl_6$  (3). (a) The unit cell showing  $RuCl_6$  and  $NaCl_6$  polyhedra connected along the c-axis. (b) Ball and stick model showing hydrogen bonds between methylammonium cations and Cl ligands. The red dotted bonds are drawn between N and Cl. (c) A perspective view of the structure showing columns of face-shared  $RuCl_6$  and  $NaCl_6$  polyhedra which are separated by MA cations.

 $^{\sim}3.34$  Å, while the shortest N···Br distances in **6-8** are  $^{\sim}3.50$  Å (**Table S2**).

In terms of the optical properties of **3** to **8**, the chlorides, **3** to **5**, show LMCT bands that are typical of isolated [RuCl<sub>6</sub>]<sup>3-</sup> ( $d^5$ ) complex ion in octahedral coordination.<sup>56,57</sup> Specifically, each of these compounds exhibits four absorption bands in the 5.50-2.25 eV (225-550 nm) range and they are red in colour (**Fig. 8**, **Table S7**). Note that the spectrum of **4** is slightly red-shifted compared to those of **3** and **5** perhaps due the role that Ag plays in LMCT for this compound. The bromides, **6** and **7** appear black and their spectra are more complex; it is therefore difficult to resolve the peaks (**Fig. S21**).

We measured the magnetic susceptibility of  $MA_2NaRuCl_6(3)$  as a typical representative of this unusual class of chain compounds. **3** has a largely temperature-independent magnetic moment, similar to the Kotani prediction for isolated low-spin  $d^5$  Ru<sup>3+</sup> ions (**Fig. 5**). Unlike the  $d^4$  Ru<sup>4+</sup> in **1**, the moment of Ru<sup>3+</sup> does not become zero at very low temperatures because the ground state is J = 3/2 rather than J = 0. However, the moment is low in comparison with the ideal Kotani behavior. We believe that this arises due to increased exchange interactions resulting from the higher connectivity between RuCl<sub>6</sub> within the face-sharing polyhedral chains. Further theoretical development of this intermediate coupling regime is a highly desirable future direction.<sup>58</sup>

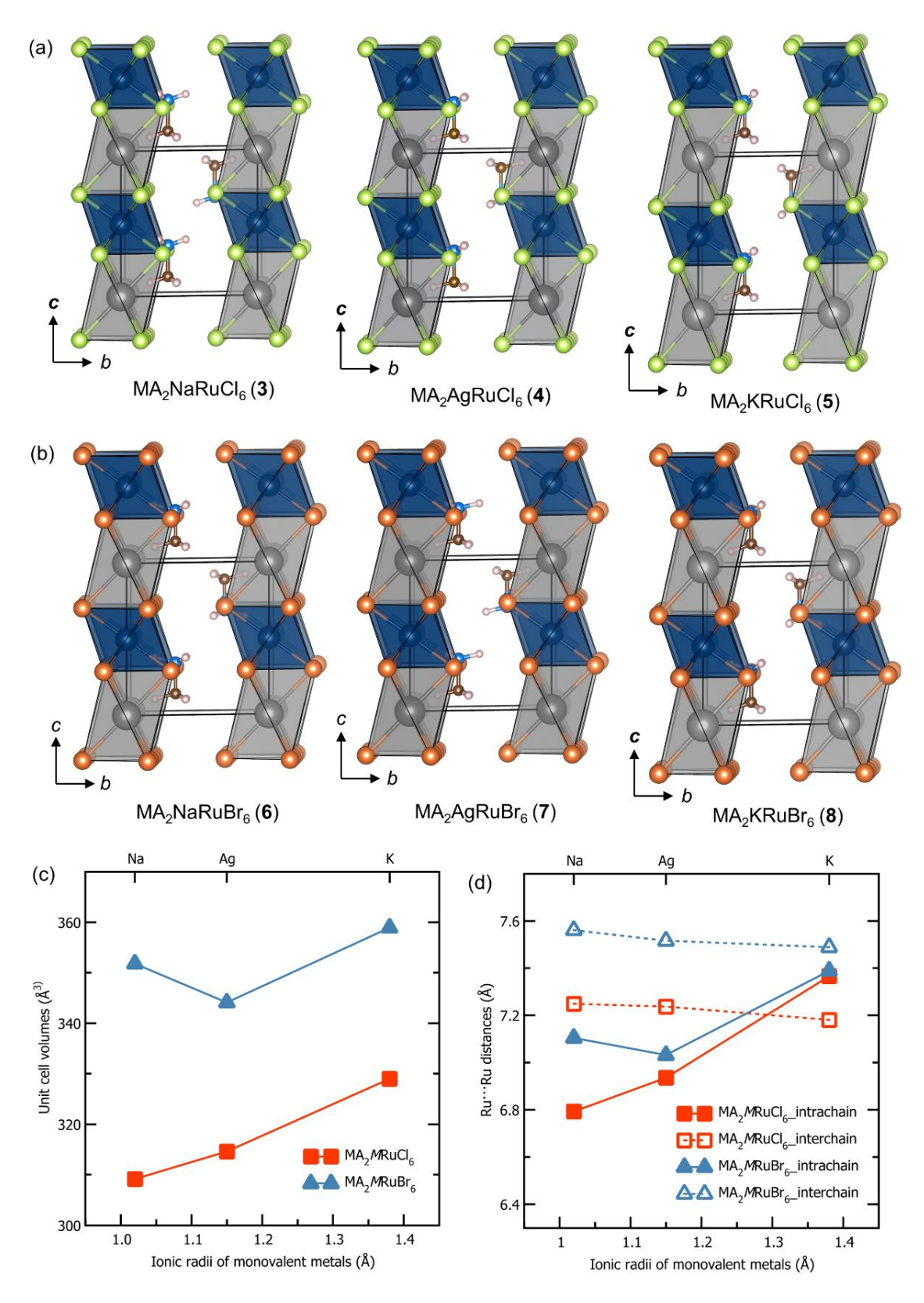


**Fig. 7.** Single-crystal X-ray structures of  $MA_2MRuX_6$  showing infinite chains of face-shared  $RuX_6$  and  $MX_6$  polyhedra. (a)  $MAMRuCI_6$ . (b)  $MA_2MRuBr_6$ . The structures are drawn on same scale for the comparison of their sizes. (c) The curves show the dependence of the unit cell volumes of **3-8** on radii of monovalent metal ions (Na, Ag and K). (d) The curves show the dependence of intra and interchain Ru···Ru distances on the radii of monovalent metal ions.

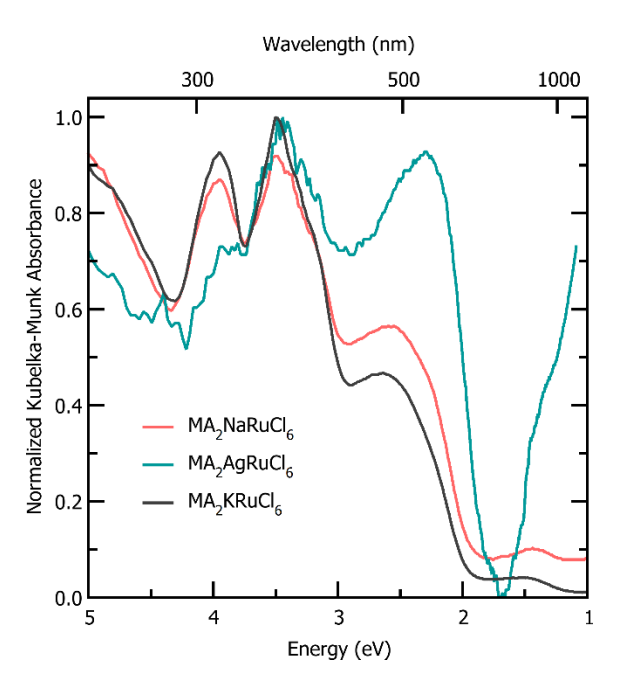
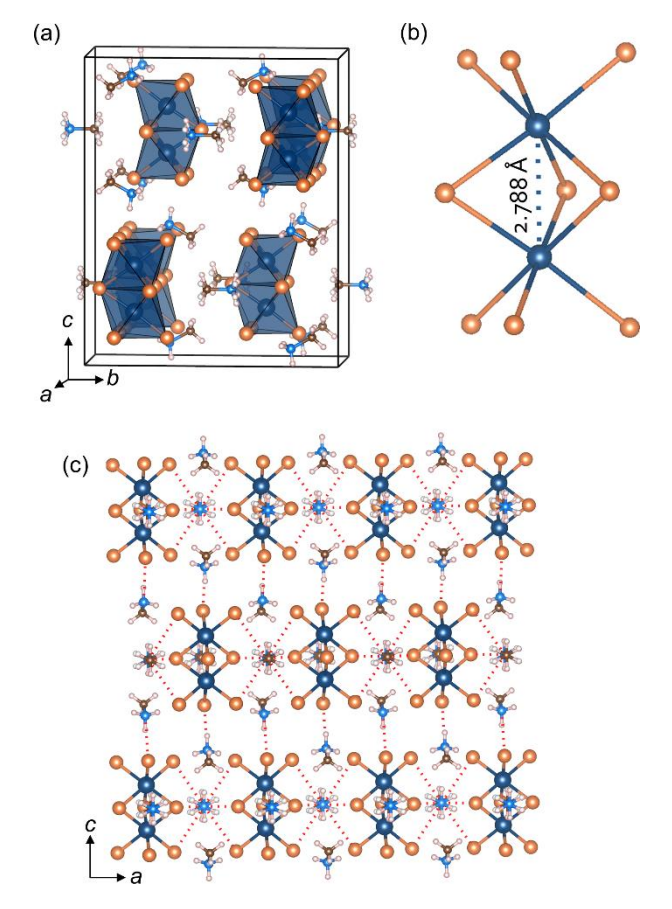


Fig. 8. Kubelka-Munk absorption spectra of  $MA_2NaRuCl_6$  (3),  $MA_2AgRuCl_6$  (4) and  $MA_2KRuCl_6$  (5).

## $[Ru_2Br_9]^{3-}$ containing dimer $MA_3Ru_2Br_9$ (9)

Several hybrid  $A_3M_2X_9$  compounds (A = monovalent organic cation; M = trivalent metal ions and X = halides) of the main group elements have been studied previously, including MA<sub>3</sub>Sb<sub>2</sub>X<sub>9</sub> (X = Br or I),<sup>59,60</sup> [C(NH<sub>2</sub>)<sub>3</sub>]<sub>3</sub> $M_2$ l<sub>9</sub> (M = Sb or Bi),<sup>61</sup> MA<sub>3</sub>Bi<sub>2</sub>X<sub>9</sub> (X = Br or I).<sup>62</sup> Some of these hybrids adopt  $A_3M_2X_9$ -type layered structures<sup>63,64</sup> of the type shown in **Fig. 1**, while others contain dimeric  $M_2X_9$ <sup>3-</sup> anions comprising two facesharing  $MX_6$  octahedra. Compound **9** contains one [Ru<sub>2</sub>Br<sub>9</sub>]<sup>3-</sup> dimer oriented along the crystallographic c-direction and two crystallographically independent methylammonium cations (**Figs. 9a, b**). One type of methylammonium cation lies in the lateral spaces between the dimers, while the other type is present at both ends of the dimers. As in the other compounds described in previous sections, the methylammonium cations form hydrogen bonds with the halide ligands (**Fig. 9c, Table S2**).

Unlike the very regular RuX<sub>6</sub> octahedra in 1 through 8, the RuBr<sub>6</sub> octahedra in **9** are slightly distorted with Br<sub>b</sub>-Ru-Br<sub>b</sub> bond angles > 90 ° and  $Br_t$ -Ru- $Br_t$  bond angles < 90 ° (b and t indicate bridging and terminal ligands, respectively) (Table S6). They also show three slightly different Ru-Br bond distances; Ru-Br<sub>b</sub>  $(2.503 \text{ Å} \times 2, 2.483 \text{ Å} \times 1)$  and Ru-Br<sub>t</sub>  $(2.493 \text{ Å} \times 2, 2.483 \text{ Å} \times 1)$ . The most striking structural feature, however, is the very short Ru···Ru distance (2.789 Å) in the  $[Ru_2Br_9]^{3-}$  dimer (Fig. 9b). This bond length is even shorter than the Ru···Ru distance in the previously reported hybrid ruthenium halide phase, [I-ethyl-3methylimidazolium]<sub>3</sub>Ru<sub>2</sub>Br<sub>9</sub>, (2.880 Å).<sup>39</sup> Both of these compounds have M···M distances that are strikingly shorter than those in the Sb and Bi mentioned earlier, which are typically around 3.3 Å, providing compelling evidence that the ruthenium compounds are exhibiting Ru-Ru bonding. There are several inorganic compounds containing the Ru<sub>2</sub>X<sub>9</sub><sup>3-</sup> dimers



**Fig. 9.** Crystal structure of  $MA_3Ru_2Br_9$  (9). (a) The unit cell. (b) The  $[Ru_2Br_9]^{3-}$  dimer. (c) 1D chains formed by hydrogen bond interactions between methylammonium and the bridging bromides. The red dotted bonds are drawn between N and Br.

that are also believed to exhibit metal-metal bonding. Because of the metal-metal interaction, Ru ions are not at the centers of their octahedra but are slightly displaced towards the center of the dimer. In light of the very high ligand field stabilization energy that would prefer to make the  $RuX_6$  units regular, we must conclude that the Ru-Ru bonding interaction is a significant stabilizing factor. This may be why the dimeric structure appears to preferred in the hybrid ruthenium compounds, rather than the layered  $A_3M_2X_9$  structure.

The optical properties of **9** reveal two intense double bands centered around 4.0 and 2.3 eV (**Fig. 10**). These bands arise from LMCT and  $\sigma \rightarrow \sigma *$  transitions and are commonly found in Ru³+ dimers with the significant metal-metal interactions. The magnetic moment of Ru³+ in MA₃Ru₂Br₃ deviates substantially from the ideal  $d^5$  Ru³+ single-ion behavior (**Fig. 5**), with a dramatically lowered, temperature-independent moment compared to the predicted Kotani behavior for low-spin  $d^5$ . This observation cannot be accounted for by changing the spin-orbit coupling constant or adjusting the background from the sample holder within reasonable limits, so we ascribe this lowering of the effective magnetic moment to metal-metal bonding within the Ru₂Br₃ dimers, as discussed above.

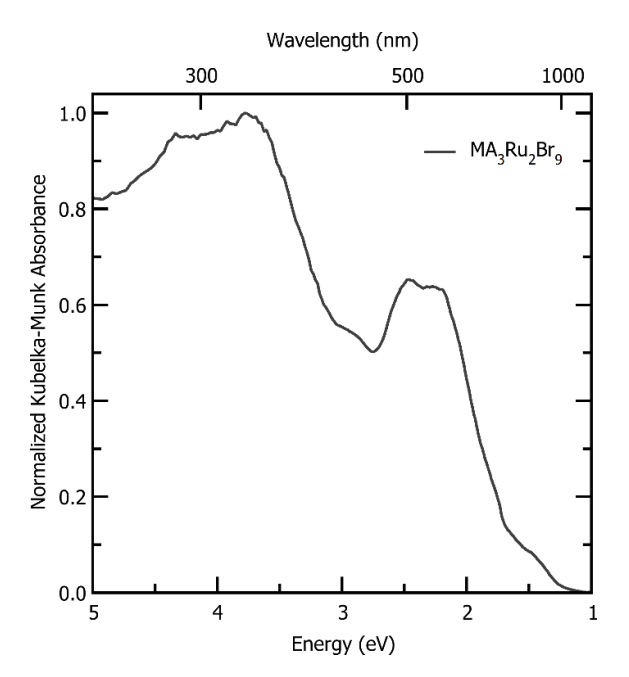


Fig. 10. Kubelka-Munk absorption spectrum of MA<sub>3</sub>Ru<sub>2</sub>Br<sub>9</sub> (9).

#### **Conclusions**

The conclusions section should come in this section at the end of the article.

## **Conflicts of interest**

There are no conflicts to declare.

# **Acknowledgements**

This work is supported by the U. S. Department of Energy, Office of Science, Basic Energy Sciences, under the SC0012541 Grant. The authors acknowledge Materials Research Science and Engineering Center (MRSEC) (Grant No. NSF DMR 1720256) for providing access to its shared facilities created at UC Santa Barbara. PV thanks the Department of Science & Technology (DST), Govt. of India for an Overseas Post-doctoral Visiting Fellowship (Fellowship Award No. JNC/AO/A.0610-1(3)/2018-03), managed by Jawaharlal Nehru Centre for Advanced Scientific Research (JNCASR), Bangalore, India.

# **Notes and references**

- 1 A. Kojima, K. Teshima, Y. Shirai and T. Miyasaka, *J. Am. Chem. Soc.*, 2009, **131**, 6050–6051.
- M. A. Green, A. Ho-Baillie and H. J. Snaith, *Nat. Photonics*, 2014, 8, 506–514.
- J. Burschka, N. Pellet, S.-J. Moon, R. Humphry-Baker, P. Gao, M. K. Nazeeruddin and M. Grätzel, *Nature*, 2013, 499, 316–319.
- 4 J.-H. Im, I.-H. Jang, N. Pellet, M. Grätzel and N.-G. Park, *Nat. Nanotechnol.*, 2014, 9, 927–932.

- 5 A. G. Kontos, A. Kaltzoglou, M. K. Arfanis, K. M. McCall, C. C. Stoumpos, B. W. Wessels, P. Falaras and M. G. Kanatzidis, *J. Phys. Chem. C*, 2018, **122**, 26353–26361.
- 6 N. K. Noel, S. D. Stranks, A. Abate, C. Wehrenfennig, S. Guarnera, A.-A. Haghighirad, A. Sadhanala, G. E. Eperon, S. K. Pathak, M. B. Johnston, A. Petrozza, L. M. Herz and H. J. Snaith, *Energy Environ. Sci.*, 2014, 7, 3061–3068.
- 7 Z. Xiao, K.-Z. Du, W. Meng, J. Wang, D. B. Mitzi and Y. Yan, J. Am. Chem. Soc., 2017, 139, 6054–6057.
- C. C. Stoumpos, C. D. Malliakas and M. G. Kanatzidis, *Inorg. Chem.*, 2013, 52, 9019–9038.
- 9 G. Laurita, D. H. Fabini, C. C. Stoumpos, M. G. Kanatzidis and R. Seshadri, *Chem. Sci.*, 2017, **8**, 5628–5635.
- A. Wang, Y. Guo, Z. Zhou, X. Niu, Y. Wang, F. Muhammad, H.
  Li, T. Zhang, J. Wang, S. Nie and Z. Deng, *Chem. Sci.*, 2019, **10**, 4573–4579.
- Z. Deng, F. Wei, S. Sun, G. Kieslich, A. K. Cheetham and P. D. Bristowe, *J. Mater. Chem. A*, 2016, 4, 12025–12029.
- F. Wei, Z. Deng, S. Sun, F. Zhang, D. M. Evans, G. Kieslich, S. Tominaka, M. A. Carpenter, J. Zhang, P. D. Bristowe and A. K. Cheetham, *Chem. Mater.*, 2017, 29, 1089–1094.
- 13 F. Wei, Z. Deng, S. Sun, F. Xie, G. Kieslich, D. M. Evans, M. A. Carpenter, P. D. Bristowe and A. K. Cheetham, *Mater. Horiz.*, 2016, **3**, 328–332.
- 14 Y.-J. Li, T. Wu, L. Sun, R.-X. Yang, L. Jiang, P.-F. Cheng, Q.-Q. Hao, T.-J. Wang, R.-F. Lu and W.-Q. Deng, RSC Adv., 2017, 7, 35175–35180.
- 15 X.-N. Hua, J.-X. Gao, X.-G. Chen, P.-F. Li, G.-Q. Mei and W.-Q. Liao, *Dalt. Trans.*, 2019, 48, 6621–6626.
- 16 P.-F. Li, W.-Q. Liao, Y.-Y. Tang, H.-Y. Ye, Y. Zhang and R.-G. Xiong, *J. Am. Chem. Soc.*, 2017, **139**, 8752–8757.
- 17 Y.-M. You, W.-Q. Liao, D. Zhao, H.-Y. Ye, Y. Zhang, Q. Zhou, X. Niu, J. Wang, P.-F. Li, D.-W. Fu, Z. Wang, S. Gao, K. Yang, J.-M. Liu, J. Li, Y. Yan and R.-G. Xiong, *Science (80-. ).*, 2017, **357**, 306–309.
- W.-Q. Liao, Y.-Y. Tang, P.-F. Li, Y.-M. You and R.-G. Xiong, J. Am. Chem. Soc., 2017, 139, 18071–18077.
- 19 H.-Y. Ye, Y. Zhang, D.-W. Fu and R.-G. Xiong, *Angew. Chemie Int. Ed.*, 2014, **53**, 11242–11247.
- 20 A. M. Elseman, A. E. Shalan, S. Sajid, M. M. Rashad, A. M. Hassan and M. Li, *ACS Appl. Mater. Interfaces*, 2018, **10**, 11699–11707.
- D. Cortecchia, H. A. Dewi, J. Yin, A. Bruno, S. Chen, T. Baikie, P.
  P. Boix, M. Grätzel, S. Mhaisalkar, C. Soci and N. Mathews,
  Inorg. Chem., 2016, 55, 1044–1052.
- 22 L. Mao, S. M. L. Teicher, C. C. Stoumpos, R. M. Kennard, R. A. DeCrescent, G. Wu, J. A. Schuller, M. L. Chabinyc, A. K. Cheetham and R. Seshadri, *J. Am. Chem. Soc.*, 2019, **141**, 19099–19109.
- I. A. Oxton, O. Knop and J. I. Duncan, J. Mol. Struct., 1977, 38, 25–32.
- 24 H. A. Evans, D. H. Fabini, J. L. Andrews, M. Koerner, M. B. Preefer, G. Wu, F. Wudl, A. K. Cheetham and R. Seshadri, *Inorg. Chem.*, 2018, **57**, 10375–10382.
- F. Funabiki, Y. Toda and H. Hosono, J. Phys. Chem. C, 2018, 122, 10749–10754.
- 26 K. Ishida, H. Mukuda, Y. Kitaoka, K. Asayama, Z. Q. Mao, Y.

- Mori and Y. Maeno, Nature, 1998, 396, 658-660.
- O. Gingras, R. Nourafkan, A.-M. S. Tremblay and M. Côté, *Phys. Rev. Lett.*, 2019, **123**, 217005.
- 28 J. Xia, W. Siemons, G. Koster, M. R. Beasley and A. Kapitulnik, *Phys. Rev. B*, 2009, **79**, 140407.
- 29 S. Woo, S. A. Lee, H. Mun, Y. G. Choi, C. J. Zhung, S. Shin, M. Lacotte, A. David, W. Prellier, T. Park, W. N. Kang, J. S. Lee, S. W. Kim and W. S. Choi, *Nanoscale*, 2018, **10**, 4377–4384.
- I. Qasim, P. E. R. Blanchard, K. S. Knight, J. Ting and B. J. Kennedy, *Dalt. Trans.*, 2019, 48, 4730–4741.
- 31 W. Witczak-Krempa, G. Chen, Y. B. Kim and L. Balents, *Annu. Rev. Condens. Matter Phys.*, 2014, **5**, 57–82.
- 32 A. Banerjee, C. A. Bridges, J.-Q. Yan, A. A. Aczel, L. Li, M. B. Stone, G. E. Granroth, M. D. Lumsden, Y. Yiu, J. Knolle, S. Bhattacharjee, D. L. Kovrizhin, R. Moessner, D. A. Tennant, D. G. Mandrus and S. E. Nagler, *Nat. Mater.*, 2016, 15, 733–740.
- 33 A. Kitaev, Ann. Phys. (N. Y)., 2006, **321**, 2–111.
- 34 S. Mashhadi, D. Weber, L. M. Schoop, A. Schulz, B. V Lotsch, M. Burghard and K. Kern, *Nano Lett.*, 2018, 18, 3203–3208.
- D. Weber, L. M. Schoop, V. Duppel, J. M. Lippmann, J. Nuss and B. V Lotsch, *Nano Lett.*, 2016, 16, 3578–3584.
- 36 R. B. Johannesen and G. A. Candela, *Inorg. Chem.*, 1963, **2**, 67–72.
- 37 A. Earnshaw, B. N. Figgis, J. Lewis and R. D. Peacock, *J. Chem. Soc.*, 1961, 3132–3138.
- 38 H. Lu, J. R. Chamorro, C. Wan and T. M. McQueen, *Inorg. Chem.*, 2018, **57**, 14443–14449.
- D. Appleby, P. B. Hitchcock, K. R. Seddon, J. E. Turp, J. A. Zora,C. L. Hussey, J. R. Sanders and T. A. Ryan, *J. Chem. Soc. Dalt. Trans.*, 1990, 1879–1887.
- 40 M. Kotani, J. Phys. Soc. Japan, 1949, 4, 293–297.
- 41 A. Earnshaw, B. N. Figgis, J. Lewis and R. S. Nyholm, *Nature*, 1957, **179**, 1121–1124.
- 42 G. M. Sheldrick, Acta Crystallogr. Sect. C, 2015, 71, 3–8.
- 43 I. Pabst, H. Fuess and J. W. Bats, *Acta Crystallogr. Sect. C Cryst. Struct. Commun.*, 1987, **43**, 413–416.
- R. Willett, H. Place and M. Middleton, J. Am. Chem. Soc., 1988, 110, 8639–8650.
- 45 T. Steiner, *Acta Crystallogr. Sect. B*, 1998, **54**, 456–463.
- A. Jabłońska-Wawrzycka, P. Rogala, S. Michałkiewicz, M.
  Hodorowicz and B. Barszcz, *Dalt. Trans.*, 2013, 42, 6092–6101.
- 47 B. N. Figgis, J. Lewis, R. S. Nyholm and R. D. Peacock, *Discuss. Faraday Soc.*, 1958, **26**, 103–109.
- 48 F. Wei, Z. Deng, S. Sun, F. Xie, G. Kieslich, D. M. Evans, M. A. Carpenter, P. D. Bristowe and A. K. Cheetham, *Mater. Horiz.*, 2016, **3**, 328–332.
- Z. Deng, F. Wei, F. Brivio, Y. Wu, S. Sun, P. D. Bristowe and A.
  K. Cheetham, J. Phys. Chem. Lett., 2017, 8, 5015–5020.
- T. T. Tran, M. A. Quintero, K. E. Arpino, Z. A. Kelly, J. R.
  Panella, X. Wang and T. M. McQueen, *CrystEngComm*, 2018,
  20, 5929–5934.
- 51 A. P. Wilkinson, A. K. Cheetham, W. Kunnman and A. Kvick, *Eur. J. Solid State Inorg. Chem.*, 1991, **28**, 453–459.
- 52 J. B. Claridge, R. C. Layland, R. D. Adams and H.-C. zur Loye, Zeitschrift für Anorg. und Allg. Chemie, 1997, 623, 1131–1134.
- S. Kawasaki, M. Takano and T. Inami, J. Solid State Chem., 1999, 145, 302–308.

- X. Wang, Y. Guo, Y. Sun, Y. Tsujimoto, Y. Matsushita and K. Yamaura, *J. Solid State Chem.*, 2013, **204**, 40–46.
- J. M. Fletcher, W. E. Gardner, A. C. Fox and G. Topping, J. Chem. Soc. A, 1967, 1038–1045.
- B. E. Bursten, F. A. Cotton and A. Fang, *Inorg. Chem.*, 1983, 22, 2127–2133.
- G. A. Heath and J. E. McGrady, J. Chem. Soc. Dalt. Trans., 1994, 3759–3767.
- G. Chen, L. Balents and A. P. Schnyder, *Phys. Rev. Lett.*, 2009, 102, 96406.
- 59 T. Kawai, E. Takao, S. Shimanuki, M. Iwata, A. Miyashita and Y. Ishibashi, *J. Phys. Soc. Japan*, 1999, **68**, 2848–2856.
- J. Zaleski, R. Jakubas, L. Sobczyk and J. Mróz, Ferroelectrics, 1990, 103, 83–90.
- 61 P. Szklarz, A. Pietraszko, R. Jakubas, G. Bator, P. Zieliński and M. Gałazka, J. Phys. Condens. Matter, 2008, 20, 255221.
- 62 M. E. Kamminga, A. Stroppa, S. Picozzi, M. Chislov, I. A. Zvereva, J. Baas, A. Meetsma, G. R. Blake and T. T. M. Palstra, *Inorg. Chem.*, 2017, 56, 33–41.
- 63 P. Szklarz, J. Zaleski, R. Jakubas, G. Bator, W. Medycki and K. Falińska, J. Phys. Condens. Matter, 2005, 17, 2509–2528.
- 64 J. Zaleski, C. Pawlaczyk, R. Jakubas and H.-G. Unruh, J. Phys. Condens. Matter, 2000, 12, 7509–7521.